Dynamic Model for an Oxygen-Staged Slagging Entrained Flow Gasifier

ARTICLE · JULY 2011

CITATIONS
6

READS
61

7 AUTHORS, INCLUDING:

Zhe Wang
Purdue University
133 PUBLICATIONS **838** CITATIONS
SEE PROFILE

Yuxin Wu
Tsinghua University
60 PUBLICATIONS **262** CITATIONS
SEE PROFILE

Junfu Lu
Tsinghua University
155 PUBLICATIONS **666** CITATIONS
SEE PROFILE

Zheng Li
Tsinghua University
139 PUBLICATIONS **1,442** CITATIONS
SEE PROFILE

energy&fuels

ARTICLE

pubs.acs.org/EF

Dynamic Model for an Oxygen-Staged Slagging Entrained Flow Gasifier

Zhiwei Yang,[†] Zhe Wang,*[,†] Yuxin Wu,[†] Jihong Wang,[‡] Junfu Lu,[†] Zheng Li,[†] and Weidou Ni[†]

[†]State Key Lab of Power Systems, Department of Thermal Engineering, Tsinghua University, Beijing, China, 100084

[‡]School of Engineering, University of Warwick, Coventry CV4 7AL, U.K.

ABSTRACT: A dynamic gasifier model including slag flow behavior simulation was established to simulate a new type of oxygen-staged gasifier recently developed in China. A reactor network model (RNM) is used to simulate the internal gas−solid reaction zone of the gasifier, in which the reactor is divided into several zones based on the understanding of the flow characteristics in the gasifier, with each zone represented by either a plug-flow reactor or a well-stirred reactor. This space division concept can provide a more reasonable temperature distribution prediction than one-dimensional models, without costing too much computational expense. In addition, a widely accepted slag layer model is used to simulate the time-varying slag accumulation and flow on the wall and the heat transfer process through the wall. Using the developed model, two kinds of oxygen-staged gasifiers were simulated: the refractory wall gasifier and the membrane wall gasifier. The RNM predictions were compared with industrial data and computational fluid dynamics (CFD) model results, and good agreement has been observed. The temperature distribution simulation results also showed that staged oxygen feeding can reduce the temperature near the main burner significantly, therefore extending the lifetime of the burner compared with that of without staged oxygen feed. Dynamic simulation results suggest that the dynamic response of the refractory wall gasifier is much slower than that of the membrane wall gasifier. In the membrane wall gasifier, the dynamic response of the syngas temperature and composition is rather fast compared to that of the wall temperature. However, for the refractory wall gasifier, the dynamic response of syngas temperature is as slow as that of the wall temperature indicating that different control strategies should be taken into account for better slag flow and syngas temperature control for these two kinds of gasifier.

1. INTRODUCTION

Entrained-flow gasification technology has many advantages such as high throughput and efficiency and freedom from higher hydrocarbons or tars in syngas. However, even after several decades of commercialization, the availability of entrained flow gasifiers is still a bottleneck for wider application. Problems such as a short lifetime of burners and refractory walls and fouling and corrosion in syngas coolers have to be addressed in order to further improve the technology. Inappropriate operation can easily lead to a blockage in the slag tap hole or even a gasifier outage. Moreover, the formation and flow of slag on the wall has a great impact on the overall dynamic characteristics of an entrained flow gasifier through the interaction with the heat transfer process. The formation and development of the slag slayer is also a key factor affecting the lifetime of gasifier walls. Therefore, in-depth understanding to the static and dynamic characteristics of gasifier including the slag layer behavior through modeling is critical and necessary for further improvements of entrained flow gasifiers' reliability and availability. Slag flow and heat transfer processes are closely linked with the flow field and temperature distribution inside gasifiers. Therefore it is necessary to model both the reaction fluid inside the reactor and the slag flow on the wall to investigate the dynamic characteristics of the slag layer.

So far, a number of gasifier models including both reaction flow and slag layer model have been established. Among them, Schoen[1] established a Shell gasifier model, in which he divided the reactor volume into combustion zone, gasification zone, and recirculation zone and used lumped parameters for each zone simulation and the whole slag layer simulation. Seggiani[2] presented a model for time-varying slag flow in the Prenflo gasifier, evaluating the temperature and syngas concentration profiles inside the reactor with a three-dimensional computation fluid dynamics (CFD) code. Bockelie et al.,[3] Benyon et al.,[4] and Li et al.[5] applied a model similar to Seggiani's to simulate the slag flow and heat transfer processes in gasifiers. Liu and Hao[6] and Ni et al.[7] both built a detailed CFD model for slag layer simulation. Kittel et al.[8] used a simplified dynamic model to study the heat transferred into the cooling screen of the GSP gasifier. Montagnaro and Salatino's slag model[9] focuses on the char−slag interaction and near-wall particle segregation, simplifying the reactor flow field as a one-dimensional plug flow. Monaghan[10] used a so-called "reactor network model" (RNM) in which a combination of plug-flow and well-stirred reactors is used to represent the flow field in a gasifier reactor, while the slag flow was simulated using a simple single layer model lumping the solid and liquid slag layer together as one solid−liquid phase.

As seen, the reaction flow models above can be classified into three categories regarding the reaction flow field simulation methods: one-dimensional models, space division models, and CFD models. One-dimensional models are a classical method for entrained flow gasifier modeling[11−13] and have been well-validated and widely accepted for predicting the temperature and

Received: May 18, 2011
Revised: July 2, 2011
Published: July 05, 2011

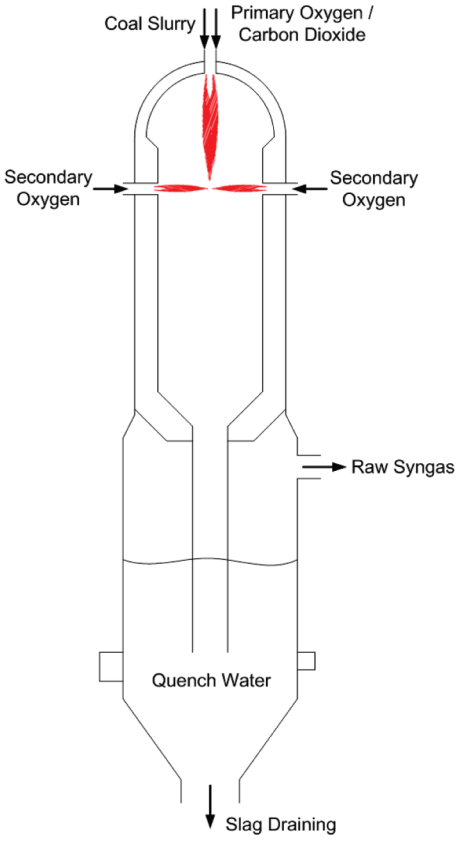

Figure 1. Schematic diagram of Tsinghua oxygen-staged gasifier.

concentration and of the syngas product. However, one-dimensional models cannot reasonably give the temperature distribution inside a gasifier, particularly for the near-wall temperature profile, which has a significant impact on slag flow behavior. On the other hand, the CFD numerical simulation method can simulate the local distribution of all parameters in such detail that it has generally been regarded as the best method for flow field steady-state simulations and has been widely applied to the gas−solid reaction flow simulations in gasifiers.[14−16] However, CFD numerical simulation usually overly taxes computational expense and is not suitable at present for dynamic simulations of the complex chemical and physical processes in a gasifier. Overall, the space division model by Schoen and Monaghan can be regarded as the best model for dynamic simulation purpose since it is a compromise approach of above two models, providing a reasonable parameter distribution inside the gasifier and avoiding large computational expense of the CFD model, while the slag layer model proposed by Seggiani can be regarded as the best among all available models in reflecting the slag layer dynamic performance since others were relatively simplified.

The aim of this paper is to develop a dynamic model based on the space-division concept and Seggiani's slag layer model to simulate the operation of new developed Tsinghua oxygen-staged gasifiers with different wall designation (refractory or membrane), for which a mixture of oxygen and carbon dioxide are injected with coal slurry into the furnace from the top burner of the gasifier, and another stream of oxygen is injected into the reactor through a secondary oxidizer burner, as shown in Figure 1. Because of the staged oxygen feeding design, the primary oxygen feeding rate going through the top burner is no longer restricted

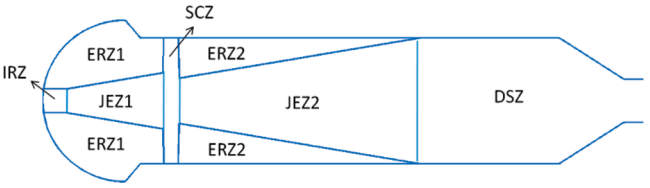

Figure 2. Schematic diagram of space division in the oxygen-staged gasifier.

to the constraint of oxygen-to-coal ratio required for partial oxidation, the intensive oxidation and high temperature environment around the top burner can be ameliorated, which can extend the burner lifetime. Meanwhile, the additional jet flow changes the limited jet flow field and enhances turbulent mixing in the staged gasifier. Currently, the refractory wall oxygen-staged gasifier has gone through the industrial demonstration stage and the membrane wall one will be demonstrated soon. Till now, not too much modeling work has been conducted on this newly developed gasifier. The purpose of the present work is to provide a dynamic numeric model to study the gasifier performance for further development of this technology.

2. MODEL DESCRIPTION

The gasifier model established in the present work comprises a reactor network model (RNM), which covers the whole internal reactor zones of the gasifier except the slag layer and a slag flow model. The two models are tightly coupled together by the mass flow rate, temperature of the slag impinging on the wall, and the heat exchange rate between the gasifier reaction zone and the slag layer. The details of the reactor network model and the slag flow model are described as below.

2.1. Reactor Network Model. *2.1.1. Space Division.* Monaghan's RNM[10] for the flow field simulation was applied in this work. The gasifier was divided into different areas according to the flow characteristics in the reactor. Each area was represented by either zero-dimensional well-stirred reactors (WSRs) or one-dimensional plug-flow reactors (PFRs) accordingly. Exact division should depend on the understanding of the flow characteristic in the reactor and the present work applied the flow field information obtained from detailed three-dimensional (3D) CFD simulations.[17]

On the basis of the vector profiles of gas velocity calculated by the CFD model, the space division was accomplished as shown in Figure 2. As shown, a mixture of feeding slurry and primary oxygen is mixed with circulated gas near the outlet of the main burner, which results in an internal recirculation zone (IRZ). And a jet expansion zone (JEZ1) is formed at the center of the reactor downward the IRZ. Surrounding the jet zone is a large external recirculation zone (ERZ1). The introduction of secondary oxygen gives rise to intensive turbulent mixing, forming a stirred combustion zone (SCZ). Under the SCZ, there is another jet expansion zone (JEZ2) and external recirculation zone (ERZ2) with the JEZ2 continuing to expand until it reaches the gasifier wall. Beneath the JEZ2 is a downstream zone (DSZ) from which syngas flows out of the gasifier.

On the basis of the flow conditions of these zones, they were characterized into WSRs and PFRs respectively as shown in Figure 3. For simplicity, all the recirculated gas in the ERZ1 was assumed to return to the JEZ1 through the IRZ zone and all the recirculated gas in the ERZ2 was assumed to return the JEZ2

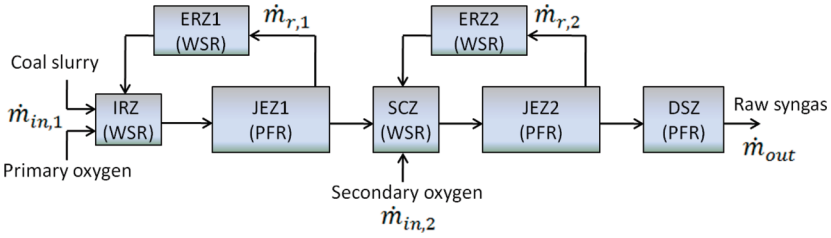

Figure 3. RNM model for the oxygen-staged gasifier.

through the SCZ. An additional simplification was made that the secondary oxygen is symmetrically introduced into the gasifier at the same height. In this model, two secondary nozzles were applied to the industrial refractory wall oxygen-staged gasifier and three to the membrane wall gasifier. The recirculation ratios α_1 and α_2 ($\alpha_1 = \dot{m}_{r,1}/\dot{m}_{\mathrm{in},1}$, $\alpha_2 = \dot{m}_{\mathrm{in},2}/(\dot{m}_{\mathrm{in},1} + \dot{m}_{\mathrm{in},2})$ were determined based on a free jet assumption,[18] $\alpha = 0.47(d_{\mathrm{gasifier}}/d_c) - 0.5$, where d_c is regarded as the inlet diameter of the jet and d_{gasifier} is the gasifier diameter.

The computational effort required for RNM is notably less than for CFD simulation. Although this model cannot fully reflect the effect of turbulent mixing on the flow field and gas−solid reactions in the way that the CFD model can, it can still obtain a reasonable distribution of parameters in the furnace, especially for the near-wall temperature distribution that has a great impact on the slag flow and heat transfer process through the wall.

2.1.2. Governing Equations for Each Zone. In setting up the governing equations for each zone, the following assumptions were made for simplification:

(1) The pressure in the reactor is kept constant.
(2) All atomized liquid drops and particles have uniform sizes.
(3) The diffusion terms in the gas conservation equation and the energy conservation equation can be ignored; as entrained flow gasifiers generally operate at elevated pressure and gas flow rate is large, convection is much stronger than diffusion.
(4) The dynamic response of the reaction and flow was regarded to be much faster than that of the slag layer and the heat transfer process through the wall.
(5) All ash content in the particles deposited on the wall enters the slag layer, but the solid carbon bounces off the wall. Therefore, carbon reactions on the surface of the slag layer were neglected.

On the basis of above assumptions, the following conservation equations can be given for a 1D PFR. Note that the same equations can be applied to WSRs, with $\partial/\partial z$ terms replaced by $1/L_{\mathrm{WSR}}$, where L_{WSR} is the length of a WSR.

Gas-phase species mass conservation equation

$$0 = -\frac{\partial F_{\mathrm{g},i}}{\partial z} + AS_{\mathrm{g},i} \tag{1}$$

where, $F_{\mathrm{g},i}$ is the mole flow rate of the ith gas species (kmol/s) (O_2, CO, CO_2, H_2, H_2O, H_2S, N_2, Ar, tar), A is the flow area (m^2), and $S_{\mathrm{g},i}$ is the chemical reaction source term for ith gas species (kmol/(m^3 s)).

Solid-phase mass conservation equation

$$0 = -\frac{\partial F_{\mathrm{p}}}{\partial z} + AS_{\mathrm{p}} - \dot{m}_{slagging} \tag{2}$$

where, F_{p} is the mass flow rate of solid particles (kg/s); S_{p} is the chemical reaction source term of solid (kg/(m^3 s)); and $\dot{m}_{\mathrm{slagging}}$ is the ash deposition rate per unit length (kg/(m s)). This term is nonzero only in zones adherent to the wall.

Carbon content mass conservation equation

$$0 = -\frac{\partial(F_{\mathrm{p}} \cdot X_{\mathrm{C}})}{\partial z} + AS_{\mathrm{C}} \tag{3}$$

where X_{C} is the mass fraction of carbon in solid particles and S_{C} is the chemical reaction source term for carbon (kg/(m^3 s)).

Gas-phase energy conservation equation

$$0 = -\frac{\partial(F_{\mathrm{g}}h_{\mathrm{g}})}{\partial z} + A(\dot{Q}_{homo} + (1 - f_Q)\dot{Q}_{hete}) + \dot{Q}_{conv,\mathrm{p}\rightarrow\mathrm{g}} - \dot{Q}_{conv,\mathrm{g}\rightarrow\mathrm{w}} \tag{4}$$

where, F_{g} is the gas phase mole flow rate (kmol/s); h_{g} is the sensible enthalpy of the gas phase (kJ/kmol); $\dot{Q}_{\mathrm{homo}}$ and $\dot{Q}_{\mathrm{hete}}$ are the heat source terms released by homogeneous reactions/water evaporation and heterogeneous reactions, respectively (kJ/(m^3 s)); $\dot{Q}_{\mathrm{conv,p}\rightarrow\mathrm{g}}$ is the convection heat source term between particles and gas phase per unit gasifier length (kJ/(m s)), while $\dot{Q}_{\mathrm{conv,p}\rightarrow\mathrm{w}}$ is the convection heat source term between gas phase and the wall. Note that only a fraction f_Q of the energy produced by heterogeneous reactions is absorbed by particles, while all energy produced by homogeneous reactions is assumed to be absorbed into gas phase. Due to the fact that the absorption coefficient for the gas phase is significantly lower than that for the particle cloud, all radiation related to the gas phase is neglected.

Solid-phase energy conservation equation

$$0 = -\frac{\partial(F_{\mathrm{p}}h_{\mathrm{p}})}{\partial z} + f_Q\dot{Q}_{hete} - \dot{Q}_{conv,\mathrm{p}\rightarrow\mathrm{g}} - \dot{Q}_{rad,\mathrm{p}\rightarrow\mathrm{w}} - \dot{Q}_{rad,\mathrm{p}\rightarrow\mathrm{p}} - \dot{m}_{slagging}h_{\mathrm{p}} \tag{5}$$

where, h_{p} is the sensible enthalpy of solid phase (kJ/kg); $\dot{Q}_{\mathrm{rad,p}\rightarrow\mathrm{p}}$ is the radiation heat source term between particles in adherent zones per unit gasifier length (kJ/(m s)), while $\dot{Q}_{\mathrm{rad,p}\rightarrow\mathrm{w}}$ is that between particles and the wall, which is meaningful only for those zones adjacent to the wall.

The chemical reaction source terms and heat transfer source terms in the above equations are determined by the following chemical reaction submodel and heat transfer submodel, respectively.

2.1.3. Chemical Reaction Submodel. The chemical reaction submodel consists of three parts: devolatilization and drying, homogeneous reactions, and heterogeneous reactions.

Table 1. Homogeneous Reaction Rate Expressions

reaction	rate expression	ref
$H_2 + 0.5O_2 \rightarrow H_2O$	under equilibrium	
$CO + 0.5O_2 \rightarrow CO_2$	under equilibrium	
$CH_4 + 2O_2 \rightarrow CO_2 + 2H_2O$	under equilibrium	
$tar + 7.5O_2 \rightarrow 6CO_2 + 3H_2O$	under equilibrium	
$CO + H_2O \leftrightarrow CO_2 + H_2$	$R = 2.75 \times 10^9 \exp(-10072/T)([CO][H_2O] - [CO_2][H_2]/K_{eq,shift})$	19
$CH_4 + H_2O \leftrightarrow CO + 3H_2$	$R = 312 \exp(-30\,000/(1.987T))[CH_4]$	20

Devolatilization and Drying. Because of the high temperature in the gasifier, drying and devolatilization are sufficiently fast (~1 ms) compared to the residence time of the particles in the IRZ; thus, rates of these processes are not calculated. Therefore, all particles are assumed to be fully dried and devolatilized before leaving the IRZ, requiring the use of drying and devolatilization source terms in the IRZ only.

During the drying process, all moisture is assumed to leave the particle upon heating, thus

$$S_{g,H_2O} = (F_{H_2O} + F_{coal}Y_{as,H_2O})/18/V_{IRZ} \quad (6)$$

$$S_p = -F_{coal}Y_{as,H_2O}/V_{IRZ} \quad (7)$$

$$\dot{Q}_{homo} = -S_{g,H_2O}h_f/V_{IRZ} \quad (8)$$

where, F_{H_2O}, F_{coal} are the mass content of water and coal in the feeding coal slurry, respectively (kg/s), Y_{as,H_2O} is the moisture content in coal on an as-received basis, and h_f is the latent heat of water (kJ/kmol).

During the devolatilization process, coal is assumed to decompose into char, CO, CO_2, H_2, H_2O, CH_4, H_2S, N_2, and tar (assumed as C_6H_6). A devolatilization model similar to that in Wen's gasifier model[12] is used to get the volatile composition and yield and the following source terms

$$S_{g,i} = F_{coal}V^*Y_{VM,i}/Mw_i/V_{IRZ} \quad (9)$$

$$S_p = -F_{coal}V^*/V_{IRZ} \quad (10)$$

where $V^*$is the volatile yield per unit mass of coal (kg/kg coal); $Y_{VM,i}$ is the mass concentration of the ith species in volatile; and Mw^i is the molar mass of the ith species (kg/kmol).

Homogeneous Reactions. The molar source term for the ith gas-phase species from homogeneous reactions is $S_{g,i} = \Sigma_n \nu_{i,n}R_n$, where R_n is the rate of the nth homogeneous reaction (kmol/(m^3 s)) and $V_{i,n}$ is the stoichiometric coefficient for the ith gas-phase species in the nth homogeneous reaction. All the homogeneous reactions considered in this work as well as their rate expressions are listed in Table 1. Note that the rates of gas phase combustion are extremely fast compared to other reactions in gasifiers; therefore, they are considered as in equilibrium. As heterogeneous reactions are rate limiting under all realistic conditions in gasifiers, this simplification does not affect the accuracy of the model.

Heterogeneous Reactions. The molar source term for the ith gas-phase specie from heterogeneous reactions is $S_{g,i} = 1/Mw^{char}\Sigma_m \nu_{i,m}R_m$, while the mass source term for the solid phase is $S_p = \Sigma_m R_m$, where R^m is the rate of the mth heterogeneous reaction (kg/(m^3 s)), $\nu_{i,m}$ is the stoichiometric coefficient for the ith gas-phase species in the mth heterogeneous reaction. Four heterogeneous reactions are considered in the work, as follows:

$$C_\alpha H_\beta O_\gamma N_\delta S_\varepsilon A + \left(\frac{\alpha}{\phi} + \frac{\beta}{4} - \frac{\gamma}{2} - \frac{\varepsilon}{2}\right)O_2 \rightarrow 2\left(1 - \frac{1}{\phi}\right)\alpha CO + \left(\frac{2}{\phi} - 1\right)\alpha CO_2 + \left(\frac{\beta}{2} - \varepsilon\right)H_2O + \varepsilon H_2S + \frac{\delta}{2}N_2 + ash \quad (11)$$

$$C_\alpha H_\beta O_\gamma N_\delta S_\varepsilon A + (\alpha - \gamma)H_2O \rightarrow \alpha CO + \left(\alpha + \frac{\beta}{2} - \gamma - \varepsilon\right)H_2 + \varepsilon H_2S + \frac{\delta}{2}N_2 + ash \quad (12)$$

$$C_\alpha H_\beta O_\gamma N_\delta S_\varepsilon A + \alpha CO_2 \rightarrow 2\alpha CO + \gamma H_2O + \left(\frac{\beta}{2} - \gamma - \varepsilon\right)H_2 + \varepsilon H_2S + \frac{\delta}{2}N_2 + ash \quad (13)$$

$$C_\alpha H_\beta O_\gamma N_\delta S_\varepsilon A + \left(2\alpha - \frac{\beta}{2} + \gamma + \varepsilon\right)H_2 \rightarrow \gamma H_2O + \alpha CH_4 + \varepsilon H_2S + \frac{\delta}{2}N_2 + ash \quad (14)$$

The unreacted-core shrinking model and kinetics used in Wen's work[12] are applied to this work for calculating the rate of these heterogeneous reactions. Note that all sulfur in the fuel was assumed to be converted into H_2S and the all nitrogen was assumed to be converted into N_2, since the quantities of these elements are relatively small and they have a negligible effect on the main syngas composition.

2.1.4. Heat Transfer Submodel. The heat source terms involved in gas-phase and solid-phase energy conservation equations include two convection source terms (gas-to-particle, gas-to-wall) and two radiation source terms (particle-to-particle, particle-to-wall). The calculating expressions of these terms are as follows:

$$\dot{Q}_{conv,p\rightarrow g} = aAh_{p\rightarrow g}(T_p - T_g) \quad (15)$$

$$\dot{Q}_{conv,g\rightarrow w} = \pi D_{gasifier}h_{g\rightarrow w}(T_g - T_w) \quad (16)$$

$$\dot{Q}_{rad,p\rightarrow w} = \pi D_{gasifier}\sigma\varepsilon_w({T_p}^4 - {T_w}^4) \quad (17)$$

$$\dot{Q}_{rad,p\rightarrow p} = \sum_i(\pi D_{zone}\sigma\varepsilon_p({T_p}^4 - {T_{p,i}}^4)) \quad (18)$$

dx.doi.org/10.1021/ef200742s |Energy Fuels 2011, 25, 3646–3656

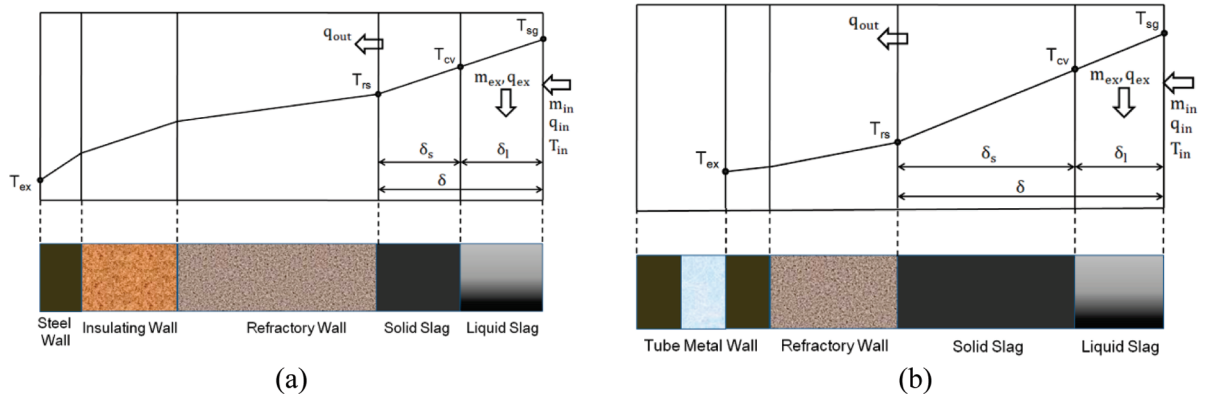

Figure 4. Illustrations of the material layers considered in the slag models of the refractory wall gasifier (a) and the membrane wall gasifier (b).

where, T_w is the slag surface temperature (K) and $T_{p,i}$ is the particle temperature in the ith adherent zone.

The Nusselt number for the two types of convection is calculated using following equations:[21,22]

$$Nu_{g\rightarrow p} = 1.32 Re_{g\rightarrow p}^{1/2} Pr^{1/3} \quad (19)$$

$$Nu_{g\rightarrow w} = 0.023 Re_{g\rightarrow w}^{0.8} Pr^{0.4} \quad (20)$$

2.2. Slag Layer Model. The slag layer model developed by Seggiani[2] was applied to simulate the time-varying slag accumulation and flow on the wall of the oxygen-staged gasifier. In this work, the molten slag was considered to be a Newtonian fluid above the temperature of critical viscosity T_{CV}, and at temperatures below T_{CV}, the slag is assumed unmovable. The temperature profile across the slag layer was assumed to be linear. Note that in nonstationary conditions, this assumption of linear temperature profile is only acceptable when the local variations of temperatures in the slag deposit are moderate.

In entrained flow gasifiers, part of the viscous ash particles carried by the gas phase deposits on the wall and solid and liquid slag layers form. For a refractory wall gasifier, the ambient temperature is local environment temperature and natural convection is accounted for between the external surface of the steel wall and the environment. For a membrane wall gasifier, the ambient temperature is set as the cooling water temperature. In this case, forced convection is considered between the internal surface of the tube metal wall and the cooling water and the cooling water temperature is kept constant (this is acceptable as long as the variations of syngas temperature in the reactor are moderate). The present work simulated both the refractory wall gasifier and membrane wall gasifier. Figure 4 illustrates the material layers considered in these two types of wall models.

The input parameters of the slag layer model from the reaction flow zone include the mass flow rate of slag impinging on the wall, the temperature of the impinging slag, and the specific heat flux from the reaction flow to slag surface. The aforementioned RNM can provide the temperature of the impinging slag and the specific heat flux to the slag flow model but cannot give the mass flow rate of slag impinging on the wall along the height of the wall, which can only be obtained from experiments or a comprehensive three-dimensional simulation of the trajectories of particles in a Lagrangian reference frame. Montagnaro[9] estimated this impinging mass flow rate along the wall using a simplified calculating expression, but the expression only applies to laboratory-scale gasifiers. The calculated impinging rate is too large for commercial-scale gasifiers. Therefore, in this work, the calculating expression was nondimensionalized and obtained:

$$\dot{m}_{slagging}(z) = 16 \dot{m}_{ash} z \exp\left(-\frac{z^*}{0.25}\right) \quad (21)$$

where $z^* = 1/L_{gasifier}$ is the dimensionless length of the gasifier ($z^* = 0$ at the top inlet of the gasifier), parameters in the equation are set to ensure that the fraction of total slag impinging to the wall in all ash content of feeding coal is consistent with industrial experience (nearly 90%).

3. DESCRIPTION OF MODEL PARAMETERS AND INPUTS

The developed model in this paper has been used to simulate two industrial oxygen-staged gasifiers, a refractory wall gasifier and a membrane wall gasifier, which are both located in Fengxi, Shanxi province, China, with the membrane wall gasifier still under construction. The geometric parameters for the two gasifiers and the division zones in the model are listed in Tables 2 and 3, respectively. Due to lack of data for the membrane wall's thickness and conductivity, values of the commercial-scale Prenflo gasifier were chosen and the geometric parameters of division zones in the refractory wall gasifier and the membrane wall gasifier were set to be the same.

The refractory wall gasifier operates at an elevated pressure of 4.0 MPa. Under normal operation conditions, the concentration of the coal slurry is 59.5%, the feed rate of coal is 26 200 kg/h, and the ratio of the mass flow rate of oxygen/coal is 0.93. These parameters were assumed to be the same for the membrane wall gasifier model due to the nonavailability of the membrane wall gasifier. The properties of feeding coal are listed in Table 4, while the main ash/slag properties used in the slag flow model are listed in Table 5.

4. RESULTS AND DISCUSSION

4.1. Steady-State Results. With the developed RNM, the global performance of the two types of oxygen-staged gasifiers is predicted and shown in Table 6. Comparisons among the present model results, CFD model results,[17] and measured data on a dry basis were listed for the refractory wall gasifier. As seen, there is good agreement among our model, the CFD model, and

Table 2. Structure Parameters of the Two Kinds of Staged Gasifiers

item	refractory wall gasifier	membrane wall gasifier
overall height (m)	7.83	7.83
gasifier inside diameter (m)	1.676	1.676
refractory wall thickness (m)	0.429	0.02
insulating wall thickness (m)	0.089	
steel/tube wall thickness (m)	0.064	0.006
refractory wall conductivity (W/(m K))	4.0	4.0
insulating brick conductivity (W/(m K))	0.9	0.9
steel/tube wall conductivity (W/(m K))	40	40

Table 3. RNM Zone Characteristics for the Staged Gasifier Model[a]

zone	characteristics
IRZ	D = 0.32 m, L = 0.32 m
JEZ1	D_{in} = 0.32 m, D_{out} = 0.75 m, L = 1.251 m, θ = 9.7°, α_r = 0.60
JEZ2	D_{in} = 0.6 m, D_{out} = 1.676 m, L = 3.15 m, θ = 9.7°, α_r = 0.81
ERZ1	V = 1.58 m^3, L = 1.571 m
ERZ2	V = 3.51 m^3, L = 3.15 m
SCZ	D = 1.676 m, L = 0.2 m
DSZ	D_{in} = 1.676 m, D_{out} = 0.58 m, L = 2.91 m

[a] D_{in} and D_{out} are the inlet and outlet diameter, respectively; L is the length; θ is the expansion angle of a jet expansion zone; and V is the volume of a zone.

Table 4. Main Properties of Shenfu Coal for the Staged Gasifier

		coal analysis for the staged gasifier			
item	V	FC	A	M	HHV (MJ/kg)
proximate analysis (%; as-received basis)	33.39	57.97	6.74	1.9	26.16

item	C	H	O	N	S	ash
ultimate analysis (%; dry basis)	74.39	4.36	13.08	0.92	0.51	6.74

Table 5. Main Properties of Coal Ash for the Staged Gasifier

item	coal ash for the staged gasifier
T_{CV} (K)	1453
viscocity η (Pa s)	$8.03 \times 10^{-8} \exp(29213/T)$
density ρ (kg/m^3)	2500
specific heat C_p (kJ/(kg K))	1.69
thermal conductivity λ (W/m/K)	1.89
emissivity σ_w	0.83

measured data for the refractory wall gasifier, partially validating the present model. In addition, as there is still no operation data nor CFD model prediction for the membrane gasifier, only RNM model prediction was given.

Table 6. RNM Model Prediction, CFD Model Prediction, and Measured Data for the Oxygen-Staged Gasifier

	T(K)	[CO]%	[CO_2]%	[H_2]%	CC(%)
refractory wall gasifier, measured data[17]	1523	45.3	19.4	34.7	96
refractory wall gasifier, CFD[17]	1511	48.9	19.6	30.8	96.1
refractory wall gasifier, RNM model	1537	41.9	20.0	35.9	95.7
membrane wall gasifier, RNM model	1507	41.3	20.4	36.0	95.4

Figure 5a and b shows the temperature distribution results of the present model for the two types of oxygen-staged gasifiers. It can be seen that after a reasonable space division using RNM, a temperature profile similar to the CFD model result[17] can be obtained: high-temperature regions are mainly located at the center jet zone and the secondary oxygen introduction zone, while low-temperature regions exist surrounding the center jet zone and also at the bottom of the furnace. Along the overall height of the gasifier, the temperature near the wall is relatively uniform. This is much different with those one-dimensional gasifier models,[11−13] in which near-wall temperature ranges from a very high value at the top to a much lower value at the bottom, and the maximum near-wall temperature was even usually higher than the failure limit temperature of the refractory wall. Moreover, the near-wall temperature profile predicted by the RNM is more reasonable, and it can provide a more solid basis for the modeling of the slag layer.

In order to investigate the influence of the staged feeding choice for oxygen, we made another calculation for the refractory wall gasifier. In the simulation, we shut down the secondary oxygen supply and had all oxygen fed into the gasifier through the main burner. The predicted temperature distribution is shown in Figure 5c. Comparing with Figure 5a, we can see that in an oxygen-staged gasifier, the temperature in the recirculating zone near the main burner is much lower than that in a nonstaged gasifier. The temperature decrease can mitigate the severe operation environment for the main burner to some extent and, therefore, extend the main burner lifetime compared with that of the nonstaged gsaifier, which is consistent with industrial experience that the lifetime of the main burner for an oxygen-staged gasifier is about 106 days while that of nonoxygen-staged General Electric (GE) gasifier is only about 60−90 days.

Figure 6 illustrates the liquid and solid slag layer thickness for the two types of oxygen-staged gasifiers. Note that lumped average parameters are used for the slag layer in those zones represented by WSRs (ERZ1, ERZ2, and SCZ).

As shown in Figure 6, the most obvious difference between these two gasifiers is that there is no solid slag layer in the refractory wall gasifier while in the membrane wall gasifier the solid slag layer is rather thick. This is due to the different structure and heat transfer characteristics of the two kinds of walls. For a refractory wall gasifier, the fire bricks are very thick and the heat exchange between the wall and the outside air is slow, resulting a large overall thermal resistance. However, for a membrane wall gasifier, the water tube wall and the refractory lining are both very thin and the heat convection between the tube and the cooling water is very high, resulting a much smaller overall thermal resistance. This difference leads to rather different temperature profiles for the two kinds of gasifiers as shown in Figure 7.

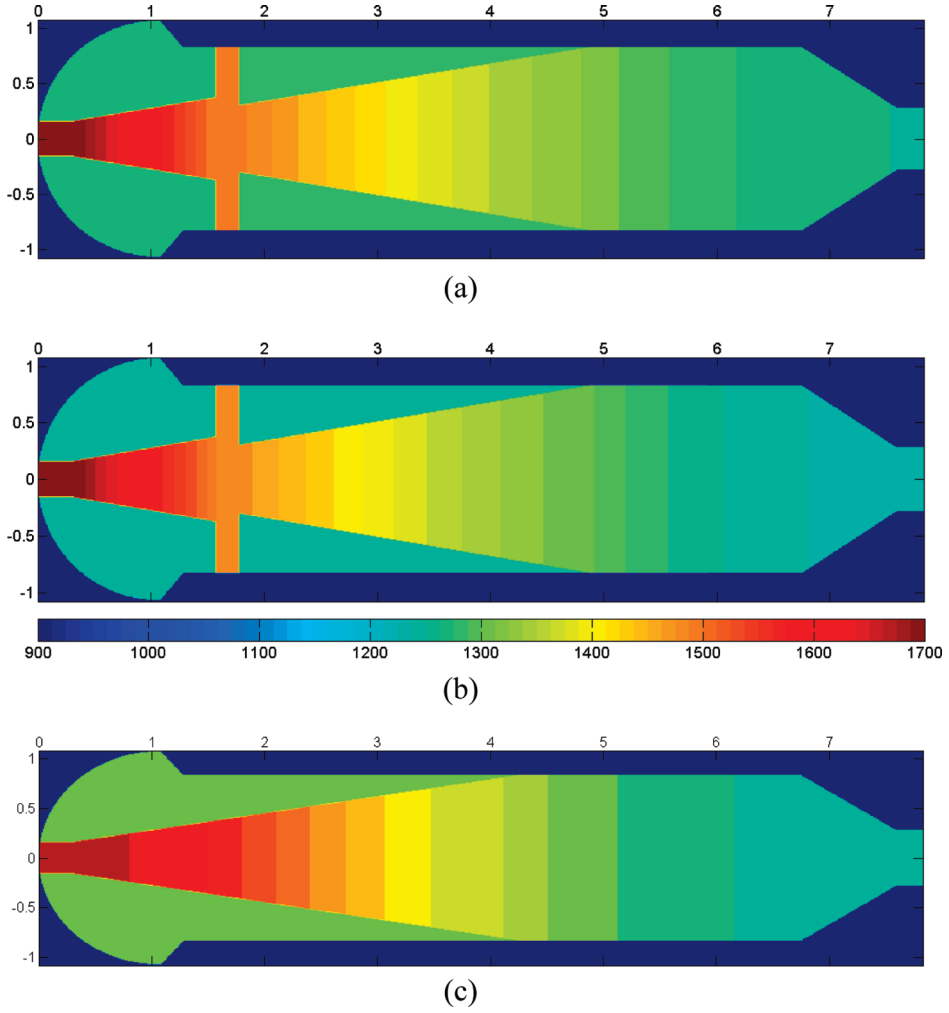

Figure 5. Temperature distribution in the gasifier: (a) refractory wall oxygen-staged gasifier; (b) membrane wall oxygen-staged gasifier; (c) nonstaged refractory wall gasifier.

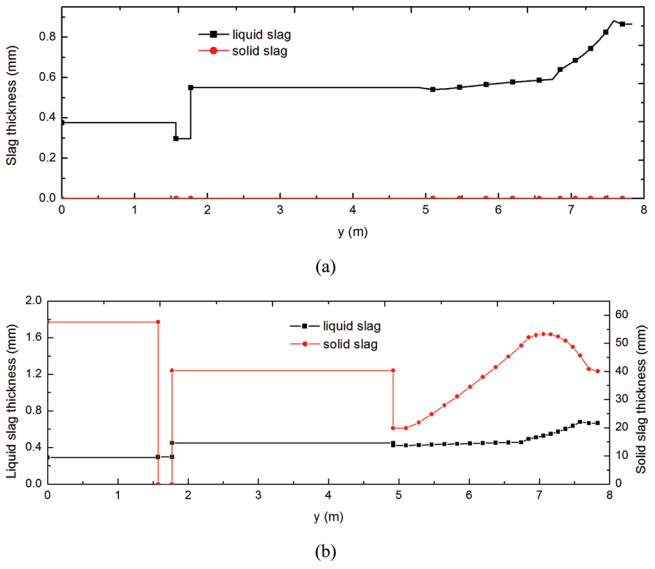

Figure 6. Solid and liquid slag layer thickness profiles for the refractory wall gasifier (a) and the membrane wall gasifier (b) ($y = 0$ at the top of the gasifier).

According to Figure 7, we can see that for the refractory wall gasifier, the temperature difference between the inner wall surface and the near-wall reaction flow is very small (about 2 °C for most of the surface area), because the thermal resistance from the reaction flow to the inner wall surface is much lower than that from the inner wall surface to the outside air. This means that the inner surface temperature is so high that no solid slag layer can form, which is also consistent with industrial applications. While for the membrane wall gasifier, the refractory lining surface temperature is much lower than the near-wall reaction flow, which provides the basis for the formation of a relatively thick solid slag layer.

Accordingly, although refractory walls are simpler in structure and cheaper than membrane walls, their lifetimes are much shorter than those of membrane walls, since refractory walls suffer from the erosion and corrosion of the flowing liquid slag directly while membrane walls are protected by a solid slag layer. This is consistent with industrial experience: the lifetime of the refractory bricks in oxygen-staged gasifiers is less than 2 years, but that of the membrane walls is usually more than 10 years. In addition, with the protection of a solid slag layer, the operation temperature for membrane wall gasifiers can be higher than that for refractory wall gasifiers, which improves the feedstock flexibility of membrane wall gasifiers.

dx.doi.org/10.1021/ef200742s |*Energy Fuels* 2011, 25, 3646–3656

But it should still be noted that in the membrane wall gasifier, the solid slag layer thickness reduces sharply in the SCZ. This can be partly explained below except for the calculation error due to the simplification made for SCZ: in this combustion zone, the flow temperature increases sharply due to additional oxygen input, enhancing the heat transfer between the syngas flow and the wall greatly; as a result, the thermal resistance from the syngas flow to the wall decreases markedly, and the temperature difference between them also decreases sharply. Hence, care needs to be taken to enhance the protection of this portion of the wall, such as increasing the thickness of the refractory lining.

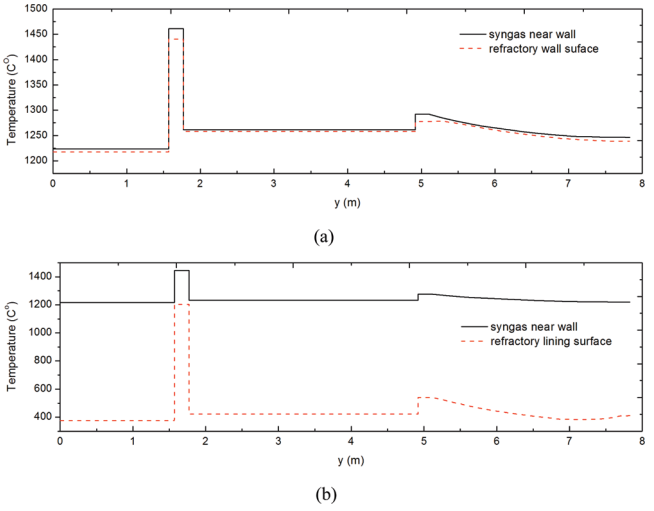

Figure 7. Temperature profiles of the internal surface of the wall and the near-wall syngas temperature for the refractory wall gasifier (a) and the membrane wall gasifier (b).

4.2. Dynamic Simulation Results. *4.2.1. Refractory Wall Gasifier.* As shown in Figure 8, when the total first stage oxygen feed rate was increased by 5%, the syngas temperature at the outlet, the major syngas species concentration, the heat flux from the syngas to the slag surface, and the liquid slag thickness experienced abrupt changes immediately. While other parameters such as the temperature of the refractory wall will change slowly due to its heat storage capacity. As the refractory wall and the slag layer temperature increase, the heat flux from the reaction flow to the slag gradually decreases due to the smaller temperature difference between them. This forces the syngas temperature and the major species concentration to keep changing but much more slowly until a balance is achieved. The change in liquid slag thickness is determined by the viscosity—temperature relationship of the slag. Higher temperatures result in lower slag viscosities, higher flow velocity, and thinner thickness.

Also, although reactions are fast and chemical equilibrium can quickly be achieved in the high temperature of the gasifier, the syngas temperature and species concentration at the outlet do not necessarily quickly reach a stable state. Figure 8a shows clearly that, after the syngas temperature increased immediately by 66 °C due to the greater amount of heat released from

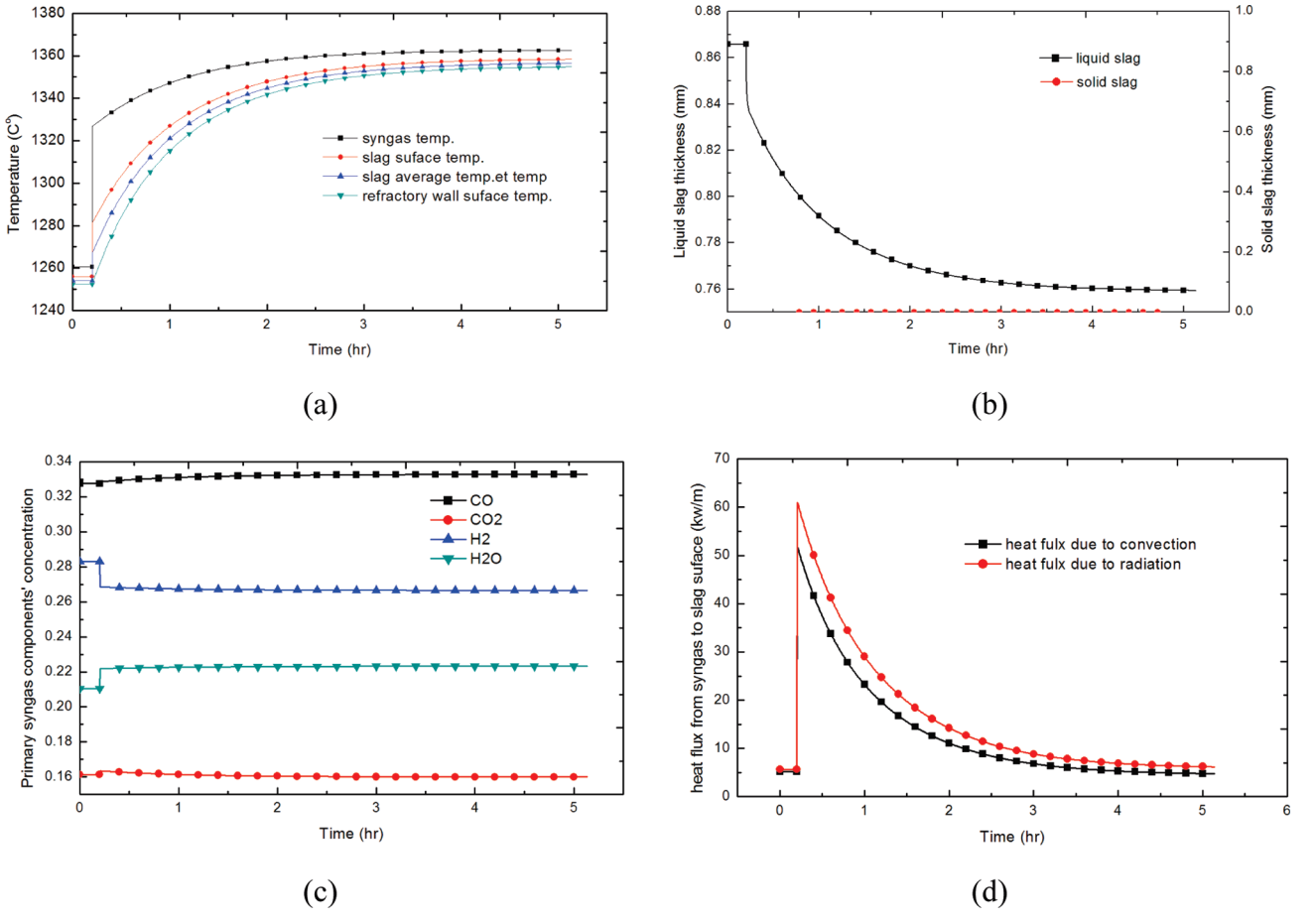

Figure 8. Dynamic response of parameters in a refractory wall oxygen-staged gasifier when total feed oxygen increases by 5%.

dx.doi.org/10.1021/ef200742s |*Energy Fuels* 2011, 25, 3646–3656

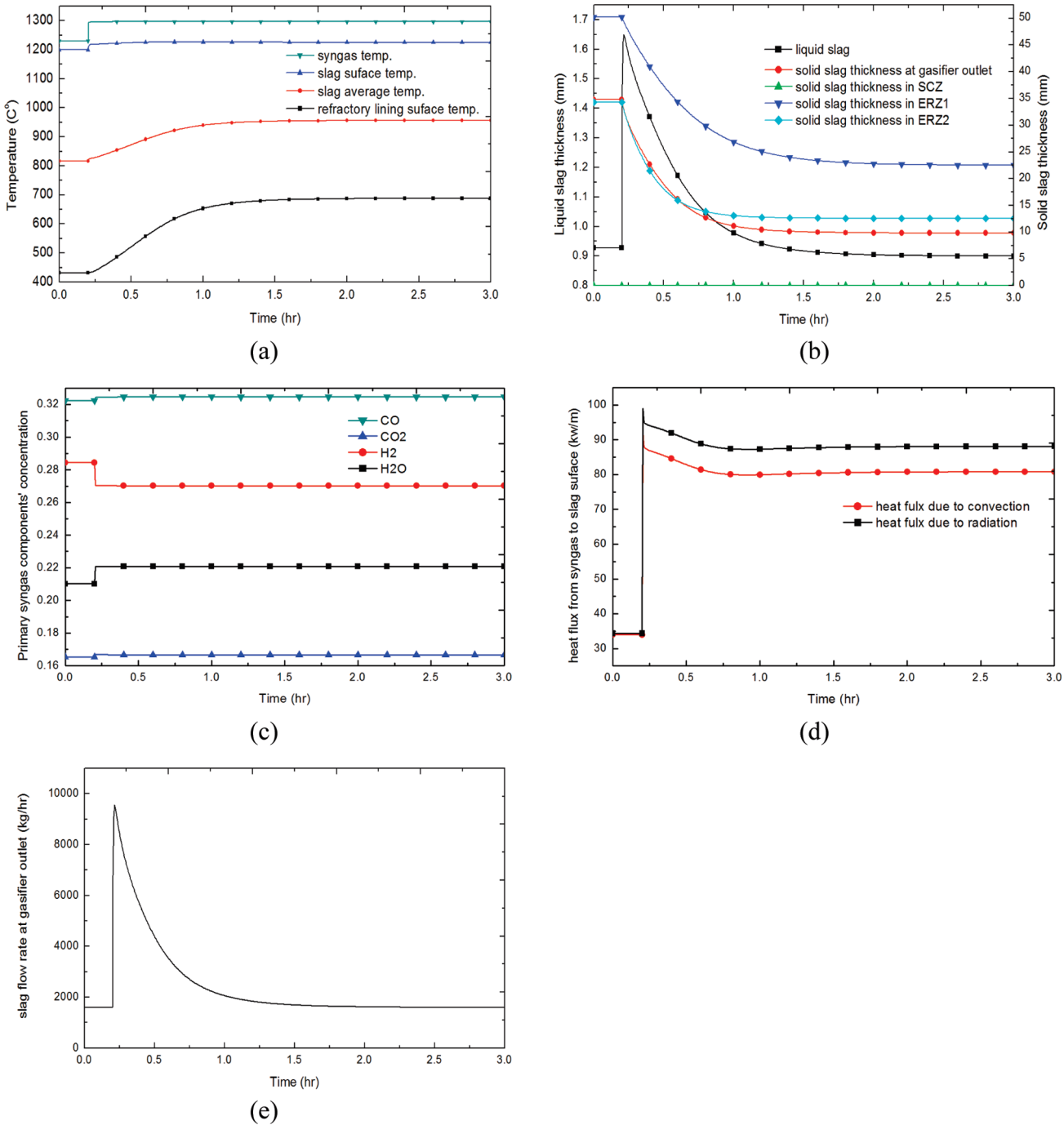

Figure 9. Dynamic response of parameters in a membrane wall oxygen-staged gasifier when total feed oxygen increases by 5%.

combustion, the syngas temperature increased more slowly (by 36 °C) over the latter 5 h due to the slow change of heat transfer process in the wall. During this time, the syngas species concentration and heating value also changed slowly.

4.2.2. Membrane Wall Gasifier. Figure 9 shows the dynamic response of parameters in a membrane wall oxygen-staged gasifier over the same step change of total feed oxygen. Similar to the phenomenon in the refractory wall gasifier, in the membrane gasifier, the syngas temperature and concentration, the heat flux from the reaction flow to the slag surface, and the liquid slag thickness in the membrane wall gasifier changed abruptly immediately. But the wall material temperature and the solid slag temperature and thickness changed slowly, which in turn affected the heat flux and the liquid slag thickness and made them change slowly.

It is worth noting that after experiencing an initial step change, the syngas temperature and the slag layer surface temperature began to remain nearly stable, unaffected by the increasing of the refractory lining surface temperature. The underlying reason for this is that when the slag layer average temperature changes, the corresponding change of solid slag thickness has an inhibition effect on the further change of the slag surface temperature. For an example, as shown in Figure 9, as the slag layer average temperature increased, part of the solid slag melted and the solid

dx.doi.org/10.1021/ef200742s |*Energy Fuels* 2011, 25, 3646–3656

slag layer became thinner, reducing the thermal resistance of the solid slag layer. This effect would not only reduce the equilibrium slag surface temperature, but also inhibit the further increase of the slag surface temperature. There was even a slight decrease in slag surface temperature, which formed an "overshooting" phenomenon. When the slag surface temperature achieved steady state, the syngas temperature and concentration would remain stable too. Therefore, the time constant for the slag surface temperature and the syngas temperature is much shorter than that for the membrane wall temperature.

Also, it should be noted that as the gasifier temperature increases, the thickness of the solid slag layer (the membrane) also decreases as shown in Figure 9b, while the refractory lining surface temperature increases. This indicates that for the membrane wall gasifier, the gasifier temperature needs to be carefully controlled to keep the slag layer thick enough to protect the membrane wall.

4.2.3. Difference between the Two Types of Walls. From the above discussion, we can see that the dynamic characteristics of the membrane wall gasifier and the refractory wall gasifier differ significantly, due to the large differences of the structure and the heat transfer properties between them.

First of all, the dynamic response speed of the membrane wall gasifier is much faster than that of the refractory wall gasifier. This is because the heat storage capacity of the membrane wall is much less than that of the refractory wall. As in Figures 8a and 9a, for the membrane wall, a stable state is achieved in about one hour, while for the refractory wall in more than five hours.

Moreover, the slag flow dynamic behavior in the membrane wall gasifier is also far different from that in the refractory wall gasifier. In the refractory wall gasifier, the liquid slag flow behavior is determined by only its temperature, while in the membrane wall gasifier, it is determined not only by its temperature but also by the phase transformation between liquid and solid slag layers, which makes the problem more complex. As shown in Figure 9b, when temperature suddenly increased, the thickness of the liquid slag layer did not decrease in spite of a lower viscosity. Instead, it increased markedly since parts of the solid slag melted to liquid slag, and the total slag flow rate leaving the gasifier also increased dramatically as shown in Figure 9e. Due to the unchanged total ash feeding rate, the thickness of the liquid slag layer then began to decrease gradually.

Besides, another difference lies on the dynamic behavior of the syngas temperature and concentration. The dynamic response of the syngas in the membrane wall gasifier is much faster than that in the refractory wall gasifier. As mentioned above, in the membrane wall gasifier, when oxygen-coal ratio changes, the temperature and major species concentration of the syngas will experience a rapid and great change first and, then, remain highly stable and nearly unchanging. However, in the case of the refractory wall gasifier, slow changes will continue to occur after the initial rapid change due to the influence of the slowly changing wall temperature. Although, when investigating the dynamic characteristics of an Integrated Gasification Combined Cycle (IGCC) or polygeneration system, the difference of the dynamic characteristics of syngas temperature and composition in these two kinds of gasifier is not large and the importance of dynamic response is still decided by the entire large system, but this should still be taken into account when designing an effective gasifier control strategy for better slag flow and syngas temperature control.

5. CONCLUSION

This paper presents a dynamic reactor network gasifier model, which includes slag flow behavior simulation in order to simulate a new type of oxygen-staged gasifier in China. On the basis of the information of the flow field calculated by a 3D CFD model, a space division method has been carried out for the oxygen-staged gasifier. In the framework of these partition zones, a reacting multiphase flow model and a slag layer model were established. Two types of oxygen-staged gasifiers (a refractory wall gasifier and a membrane wall gasifier) were simulated. The syngas prediction data under normal operation conditions agrees well with the industrial data. Furthermore, the calculated temperature distribution in the gasifier is similar to CFD model results: the high temperature region locates mainly at the center of the reactor, and near-wall temperature is lower and almost uniform along the gasifier. This temperature profile is more reasonable than that predicted by classical one-dimensional models, and can provide a more accurate basis for the calculation of heat transfer between the reaction flow and the slag layer. Comparison of temperature distribution between the oxygen-staged gasifier and a nonstaged gasifier showed that staged oxygen feeding can reduce the temperature in the recirculating zone near the main burner significantly, which can, to some extent, explain why the lifetime of the main burner of the oxygen-staged gasifier is longer than that of a nonstaged gasifier .

With this model, several dynamic simulation tests were conducted to investigate the dynamic response of the two kinds of oxygen-staged gasifier. When total feeding oxygen increases by 5%, simulation results revealed significant differences between the refractory wall gasifier and the membrane wall gasifier in their dynamic characteristics. For the refractory wall gasifier, the dynamic response is rather slow, due to the great heat storage capacity of the thick refractory bricks and insulating layer. The slowly changing refractory temperature will in turn affect the syngas temperature and concentrations, making them change slowly after the initial rapid change. Also, the equilibrium heat flux through the wall reaches close to its initial value before the step change. As to the membrane wall gasifier, the dynamic response of the slag flow is much faster than that in the refractory wall gasifier, and the temperature and the species concentration of the syngas nearly has no following features to the slag layer temperature after an initial rapid change. And, the equilibrium heat flux through the wall differs significantly from its initial value before the step change, due to a large change of solid slag layer thickness. The different dynamic characteristics of the two types of gasifier means that distinguished treatments have to be used when designing control strategies for gasifiers.

The present work carried out preliminary studies on the dynamic characteristics of the slag flow in oxygen staged gasifiers. More simulation tests will be carried out to investigate the slag dynamic behavior and the heat transfer processes under other possible operation changes in detail. Besides, great simplification has been made on the deposition mechanism of the particles to the wall, and the carbon reactions on the wall are not considered. In further studies, the detailed movement of particles in the gasifier and the char−slag interaction will be investigated using experimental methods and CFD model, in order to further improve the dynamic model.

AUTHOR INFORMATION

Corresponding Author

*Telephone: +86 10 62795736. Fax: +86 10 62795736. E-mail: zhewang@tsinghua.edu.cn.

■ ACKNOWLEDGMENT

The work is sponsored by the National Key Basic Research Development Program of China (973) under contract 2010-CB227006 and National Science Foundation of China (NSFC) under Grant 51010143.

■ NOMENCLATURE

a = contact area between solid and gas per unit volume of reactor (m^2/m^3)
A = flow area (m^2)
$D_{gasifier}$, D_{zone} = diameter of gasifier and partition zone, respectively (m)
f_Q = fraction of energy absorbed by particles in total energy produced by heterogeneous reactions
F_{H_2O}, F_{coal} = mass content of water and coal in the feeding coal slurry, respectively (kg/s)
F_g, F_p = mole flow rate of gas (kmol/s) and solid particles (kg/s), respectively
h_f = the latent heat of water (kJ/kmol)
h_g, h_p = sensible enthalpy of gas phase (kJ/kmol) and solid phase (kJ/kg)
h = convection heat transfer coefficient ($kJ/m^2/K$)
$\dot{m}_{ash}$ = flow rate of total ash entering the gasifier (kg/s)
$\dot{m}_{slagging}$ = ash deposition rate per unit length of the gasifier wall (kg/(m s))
Mw^i = molar mass of the ith species (kg/kmol)
Nu = Nusselt number
Pr = Prandtl number
$\dot{Q}$ = heat source term released by evaporation or reactions ($kJ/(m^3\ s)$)
$\dot{Q}_{conv}$ = convection heat source term per unit length (kJ/(m s))
$\dot{Q}_{rad}$ = radiation heat source term per unit length (kJ/(m s))
Re = Reynolds number
R = rate of reaction ($kg/(m^3\ s)$)
S_C, S_g, S_p = reaction source for carbon ($kg/(m^3\ s)$), gas ($kmol/(m^3\ s)$), and solid ($kg/(m^3\ s)$), respectively
T = temperature (K)
V^* = volatile yield per unit mass of coal (kg/kg coal)
v = stoichiometric coefficient in reactions
X_C = mass fraction of carbon in solid particles
Y_{as,H_2O} = moisture content in coal on an as-received basis
$Y_{VM,i}$ = mass concentration of the ith species in volatile
z = lenth of a partition zone (m)
z^* = dimensionless length of the gasifier
σ = Stefan−Boltzmann constant ($kJ/(m^2\ K^4\ s)$)
ε = emissivity

Subscripts

g = gas phase
i = the ith gas species
homo = homogeneous reactions/water evaporation
hete = heterogeneous reactions
m = the mth heterogeneous reaction
n = the nth homogeneous reaction
p = solid phase
w = gasifier wall
p → g = between particles and gas phase
g → w = between gas phase and the wall
p → p = between particles in adherent zones
p → w = between particles and the wall

■ REFERENCES

(1) Schoen, P. Dynamic modeling and control of integrated coal gasification combined cycle units. PHD thesis, Delft University of Technology, 1993.
(2) Seggiani, M. Modelling and simulation of time varying slag flow in a Prenflo entrained-flow gasifier. *Fuel* **1998**, *77* (14), 1611–1621.
(3) Bockelie, M.; Denison, K.; Chen, Z.; Linjewile, T.; Senior, C.; Sarofim, A. CFD modeling for entrained flow gasifiers in Vision 21 systems. *Presented at the Pittsburgh Coal Conference*, Pittsburgh, PA, Sept 2002; http://www.reaction-eng.com.
(4) Benyon, P. *Computational modelling of entrained flow slagging gasifiers*. PHD thesis, University of Sydney, 2002.
(5) Li, B.; Brink, A.; Hupa, M. Simplified Model for Determining Local Heat Flux Boundary Conditions for Slagging Wall. *Energy Fuels* **2009**, *23* (7), 3418–3422.
(6) Liu, S.; Hao, Y. Numerical study on slag flow in an entrained-flow gasifier. *ASME International Mechanical Engineering Congress and Exposition*, Washington, DC, Nov 11−15, 2007.
(7) Ni, J.; Zhou, Z.; Yu, G.; Liang, Q.; Wang, F. Molten Slag Flow and Phase Transformation Behaviors in a Slagging Entrained-Flow Coal Gasifier. *Ind. Eng. Chem. Res.* **2010**, *49*, 12302–12310.
(8) Kittel, J.; Hannemann, F.; Mehlhose, F.; Heil, S.; Meyer, B. Dynamic modelling of the heat transfer into the cooling screen of the SFGT-Gasifier. *Proceedings of the 7th Modelica Conference*, Como, Italy, 2009; The Modeli Association, p 326.
(9) Montagnaro, F.; Salatino, P. Analysis of char-slag interaction and near-wall particle segregation in entrained-flow gasification of coal. *Combust. Flame* **2010**, *157* (5), 874–883.
(10) Monaghan, R. F. D. *Dynamic reduced order modeling of entrained flow gasifiers*. PHD thesis, Massachusetts Institute of Technology, 2010.
(11) Ubhayakar, S.; Stickler, D.; Gannon, R. Modelling of entrained-bed pulverized coal gasifiers. *Fuel* **1977**, *56* (3), 281–291.
(12) Wen, C.; Chaung, T. Entrainment coal gasification modeling. *Ind. Eng. Chem. Process Des. Dev.* **1979**, *18* (4), 684–695.
(13) Vamvuka, D.; Woodburn, E.; Senior, P. Modelling of an entrained flow coal gasifier. 1. Development of the model and general predictions. *Fuel* **1995**, *74* (10), 1452–1460.
(14) Chen, C.; Horio, M.; Kojima, T. Numerical simulation of entrained flow coal gasifiers. Part I: modeling of coal gasification in an entrained flow gasifier. *Chem. Eng. Sci.* **2000**, *55* (18), 3861–3874.
(15) Choi, Y.; Li, X.; Park, T.; Kim, J.; Lee, J. Numerical study on the coal gasification characteristics in an entrained flow coal gasifier. *Fuel* **2001**, *80* (15), 2193–2201.
(16) Watanabe, H.; Otaka, M. Numerical simulation of coal gasification in entrained flow coal gasifier. *Fuel* **2006**, *85* (12−13), 1935–1943.
(17) Wu, Y.; Zhang, J.; Smith, P.; Zhang, H.; Reid, C.; Lv, J.; Yue, G. Three-Dimensional Simulation for an Entrained Flow Coal Slurry Gasifier. *Energy Fuels* **2010**, *24* (2), 1156–1163.
(18) Beer, J.; Chigier, N. *Combustion aerodynamics*; Applied Science Publishers: London, 1972.
(19) Jones, W.; Lindstedt, R. Global reaction schemes for hydrocarbon combustion. *Combust. Flame* **1988**, *73* (3), 233–249.
(20) Zahradnik, R. L.; Grace, R. *Chemistry and physics of entrained coal gasification*; Advances in Chemistry Series; American Chemical Society: Washington, DC, 1973; No. 131, p 126.
(21) Mills, A. *Heat Transfer*, second ed.; Prentice Hall Inc.: Upper Saddle River (NJ), 1999.
(22) Incropera, F. P.; Dewitt, D. P. *Fundamentals of Mass and Heat Transfer*; John Wiley & Sons: New York, 2002.